On the other hand, it has been shown, in the case of aryl halides, and rationalized on quantum chemical grounds that $\Delta G_c^{\ddagger}$ is roughly correlated with $E^{\circ}_{ArNu/ArNu^{\bullet -}}$.[18] Thus, when passing from one Ar$^{\bullet}$ to the other

$$\Delta\Delta G_c^{\ddagger} \simeq \alpha F \Delta E^{\circ}_{ArNu/ArNu^{\bullet -}}$$

should hold approximately. It follows that

$$\Delta\Delta G_f^{\ddagger} \simeq \Delta\Delta G^{\circ}_{ArNu} - (1 - \alpha) F \Delta E^{\circ}_{ArNu/ArNu^{\bullet -}}$$

Since ΔG°_{ArNu} is expected not to vary very much in the series, we end up with, as a rule of thumb, the more positive the standard potential of the ArNu/ArNu$^{\bullet -}$ couple the faster reaction 2.

It is seen (Table I) that this rule is approximately obeyed in the present case. In particular, this explains why the phenyl radical exhibits the lowest reactivity in the series, as with the other nucleophiles.[3g,h] Similarly, the low reactivity of the naphthyl radical is related to the fact that it is not activated by an electron-withdrawing group in contrast with the other members of the series. Two significant exceptions to the rule are the 2-quinolyl and the 2-cyanophenyl radicals. The low reactivity of the former, which was also noted with the other three nucleophiles,[3g] can be ascribed to the electronic repulsion between the lone electrons pair of the adjacent nitrogen and the electrons of the C–Nu bond as discussed earlier.[3g] The 2-cyanophenyl radical exhibits a remarkably high reactivity. We have no unequivocal explanation of this fact at present. One possibility is that the NaCN ion pair could participate in the reaction, in this case, in contrast with the other aryl radicals, since transfer of the charge through the phenyl ring on the adjacent cyano group could help the dissociation of the ion pair in the transition state. This clearly calls for experimental verification in the context of a systematic study of the effect of ion pairing evoked earlier.

(18) (a) Andrieux, C. P.; Savéant, J. M.; Zann, D. *Nouv. J. Chim.* **1984**, *8*, 107. (b) Andrieux, C. P.; Savéant, J. M.; Su, K. B. *J. Phys. Chem.*, in press.

Experimental Section

The electrochemical instrumentation and the procedures for the work in liquid ammonia were the same as previously described.[3g] The reference electrode was an Ag/Ag$^+$ 0.01 M electrode. The working electrode was either a gold disk (0.5-mm diameter), a platinum disk (0.5-mm diameter), or a mercury drop hanged to a 0.5-mm diameter gold disk as indicated in Table I.

Registry No. Phenyl radical, 2396-01-2; 1-naphthyl radical, 2510-51-2; 2-cyanophenyl radical, 95936-64-4; 3-cyanophenyl radical, 95936-65-5; 4-cyanophenyl radical, 56263-67-3; 2-quinolyl radical, 54978-39-1; 4-benzoylphenyl radical, 59922-54-2; 4-quinolyl radical, 54978-41-5; chlorobenzene, 108-90-7; diphenyl sulfide, 139-66-2; 1-chloronaphthylene, 90-13-1; 2-chlorophenylnitrile, 873-32-5; 3-chlorophenylnitrile, 766-84-7; 4-bromophenylnitrile, 623-00-7; 4-chlorophenylnitrile, 623-03-0; 2-bromoquinoline, 2005-43-8; 4-benzoylphenyl bromide, 134-85-0; 4-bromoquinoline, 611-35-8; sodium cyanide, 143-33-9; cyanide ion, 57-12-5; benzonitrile, 100-47-0; 1-cyanonaphthalene, 86-53-3; 1,2-dicyanobenzene, 91-15-6; 1,3-dicyanobenzene, 626-17-5; 1,4-dicyanobenzene, 623-26-7; 2-cyanoquinoline, 1436-43-7; 4-benzoylbenzonitrile, 1503-49-7; 4-cyanoquinoline, 2973-27-5; benzonitrile radical anion, 34478-18-7; 1-cyanonaphthalene radical anion, 34478-12-1; 1,2-dicyanobenzene radical anion, 34536-45-3; 1,3-dicyanobenzene radical anion, 34536-46-4; 1,4-dicyanobenzene radical anion, 34536-47-5; 2-cyanoquinoline radical anion, 75892-92-1; 4-benzoylbenzonitrile radical anion, 60466-04-8; 4-cyanoquinoline radical anion, 68271-78-3.

Structure and Reactivity of Thiophosphoranyl Radicals. A Quantum Chemical Study

Danielle Gonbeau,[†] Marie-Françoise Guimon,[†] Jean Ollivier,[‡] and Geneviève Pfister-Guillouzo*[†]

Contribution from the Laboratoire de Physico-Chimie Moléculaire UA 474, Université de Pau et des Pays de l'Adour, 64000 Pau, France, and the Centre de Recherche Elf-Aquitaine, Lacq, 64170 Artix, France. *Received November 13, 1985*

Abstract: Various optimized geometries were calculated for the $(PH_3SH)^{\bullet}$ radical by using the unrestricted Hartree–Fock method with a 4-31G basis set and d polarization orbitals. The $(PH_3SH\text{-}e)^{\bullet}$ form resembling a trigonal-bipyramidal structure with missing equatorial substituent (TBP-e) was the minimum energy structure. It appears that a σ^* arrangement is not stable but leads to dissociation. A potential surface for $PH_3 + SH^{\bullet} \rightarrow (PH_3SH)^{\bullet}$ indicates a preferred attack where the incoming $SH^{\bullet}$ enters an equatorial position. The pathways of dissociation into PH_3 and $SH^{\bullet}$ are described, and the transition states are calculated. This approach was generalized with OH ligands: the results show identical behavior.

1. Introduction

The promoter role of phosphite in the photosynthesis of thiols by thiyl radical trapping is a well-known experimental fact.[1] The interpretation of the mechanisms involved is controversial, especially since the results of both experimental and theoretical work for the last 15 years have led to contradictory conclusions concerning both the structure of the radicals and their possibilities of further reaction.

A trigonal-bipyramid structure with missing equatorial ligand (TBP-e) was initially proposed as being energetically favorable for these radicals. These conclusions were based on the values of ^{31}P hyperfine isotropic couplings obtained with ESR in liquid phase and on the results of several theoretical studies.[2-6]

The recent development of anisotropic ESR coupled with X-ray diffraction has generated results causing prior findings to be reconsidered. Thus, the possibility of structures different from

[†] Université de Pau.
[‡] Société Nationale Elf-Aquitaine.

(1) Loutman, R. P. US Patent 3 050 452, 1960. Wagner, P. US Patent 3 338 810, 1964. Warner, P. F. US Patent 3 567 658, 1968. Ollivier, J. US Patent 4 233 128, 1980.
(2) Davies, A. G.; Griller, D.; Roberts, B. P. *J. Chem. Soc., Perkin Trans. 2* **1972**, 993.
(3) Krusic, P. J.; Mahler, W.; Kochi, J. L. *J. Am. Chem. Soc.* **1972**, *94*, 6033.
(4) Watts, G. B.; Griller, D.; Ingold, K. U. *J. Am. Chem. Soc.* **1972**, *94*, 8784.
(5) Higuchi, J. *J. Chem. Phys.* **1969**, *50*, 1001.
(6) Fessenden, R. W.; Schuler, R. J. *J. Chem. Phys.* **1966**, *45*, 1845.

0002-7863/86/1508-4760$01.50/0

TBP-e has been envisioned, according to the nature of the ligands.[7-12]

In light of current experimental data, the two most frequently invoked structures are the trigonal bipyramid with missing equatorial ligand and the tetrahedral structure, with all possible intermediates according to the nature of the ligands. Nonetheless, there are relatively few data available on phosphoranyl radicals with SR ligands.[12-15] The ESR spectrum of $(MeSP(OEt)_3)^{\bullet}$[14] could not be utilized because of poor resolution. Attempts to characterize the species $(RSPF_3)^{\bullet}$ and $(RSPH_3)^{\bullet}$ by Giles and Roberts,[15] using RSSR photolysis in the presence of PF_3 or PH_3, were unsuccessful. Only work on $(RSPMe_3)^{\bullet}$ enabled these authors to suggest that the methyl groups had identical environments, implying a σ^*(P–S) structure or a nonequivalence (TBP-type structure) with rapid exchange of ligands.[15]

In view of the absence of data on this type of radical, we undertook a detailed theoretical study of the model entity $(PH_3SH)^{\bullet}$. In addition, the $(XPH_3)^{\bullet}$ (X = F and Cl) radicals had been the subject of only several quantum chemical approaches, which a priori favored certain types of structures.[16] The determination of the main critical points of the potential energy hypersurface of the $PH_3 + SH^{\bullet}$ system enabled us to analyze the mechanism of formation and the further reaction possibilities of the $(PH_3SH)^{\bullet}$ radical. In order to measure the modifications induced by the introduction of a sulfur-containing ligand, we first examined the $(PH_4)^{\bullet}$ radical, for which the most recent theoretical work[16,17] involved different approaches. Howell and Olsen[17] characterized the TBP-e form as a minimum, but the TBP-a form was not completely optimized, whereas Janssen et al.[16] determined minimal structures within C_{3v} constraint. Furthermore, these authors analyzed the reaction $PH_3 + H^{\bullet} \rightarrow (PH_4)^{\bullet}$ and concluded on an approach of $H^{\bullet}$ in the LUMO direction of PH_3, while Howell presented this approach as a high-energy zone. These conclusions probably arose from different symmetry constraints imposed by these authors in their respective approaches and from the fact that the d orbitals of phosphorus were not taken into consideration. We thus decided to define the importance of these two factors.

Finally, we verified that our conclusions could be generalized to the $(P(OH)_3SH)^{\bullet}$ radical, a representative compound of the environment of different phosphites used as promoters in mercaptan photosynthesis.

2. Computational Details

The calculations were performed with the MONSTERGAUSS program. The split valence 4-31G basis set was used, augmented by one set of d polarization functions on phosphorus and sulfur ($\zeta_P^d = 0.57$, $\zeta_S^d = 0.846$).[18] The open-shell states were computed by using the unrestricted Hartree–Fock procedure.

The molecular geometries were fully optimized with respect to all bond lengths and bond angles by the Broyden–Fletcher–Goldfard–Shanno gradient method.[19] The detection of transition states was carried out by employing the Powell algorithm.[20] The stationary points were characterized by force constant analysis (number of negative eigenvalues). This analysis was performed at a SCF level because of the important size of the calculations for $(PH_3SH)^{\bullet}$ and $(P(OH)_3SH)^{\bullet}$.

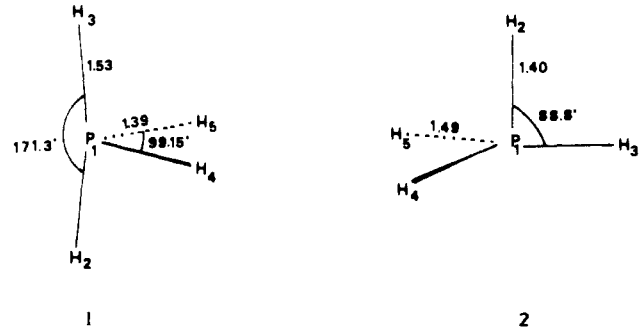

Figure 1. Optimized geometries for $PH_4^{\bullet}$ (bond lengths in Å).

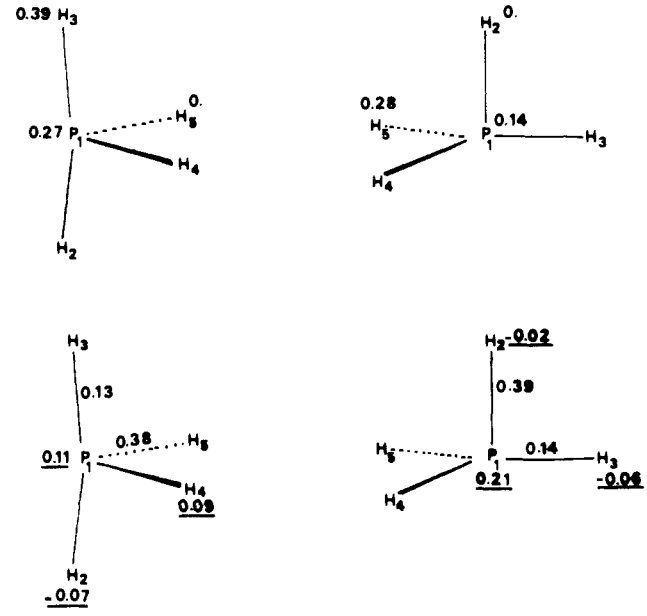

Figure 2. Valence orbital spin densities and Mulliken populations (net charges underlined) of $PH_4^{\bullet}$ radicals.

3. Geometric and Electronic Structures of $(PH_4)^{\bullet}$ and $(PH_3SH)^{\bullet}$ Radicals

3.1. $(PH_4)^{\bullet}$ Radical. We considered for this radical the three structures usually invoked on the experimental and theoretical levels: (i) the tetrahedral structure; (ii) the two structures deduced from the trigonal bipyramid with missing ligand, either in the equatorial (C_{2v} symmetry) or apical position (C_{3v} symmetry). No symmetry constraint was imposed in the minimization process.

Problems of calculation convergence were encountered for the tetrahedral structure, and no stable minimum could be determined. The lowest energy obtained was −342.480 hartrees (P–H = 1.45 Å, HPH = 110.5°) far from those determined for the other two symmetry forms: TBP-e (form **1**) = −342.5801 hartrees ($\langle S^2 \rangle$ = 0.7809), TBP-a (form **2**) = −342.5503 hartrees ($\langle S^2 \rangle$ = 0.7814).

Form **1** thus appears to be energetically favored over form **2** by about 78 kJ·mol^{-1}. This stabilization is due to electronic factors and not polar effects. In addition, the determination of the eigenvalues of the second derivative matrix showed that although form **1** indeed corresponded to a minimum, form **2** was in fact a "top hill" (two negative eigenvalues: −1.23, −0.55). It should be noted that, without characterizing it precisely, Howell[17] depicted this structure as a high-energy intermediate participating in the pseudorotation of the TBP-e form (Figure 1).

The minimized geometric parameters differ from those of Howell and Janssen, since these authors did not take the d orbitals

(7) Hamerlinck, J. H. H.; Schipper, P.; Buck, H. M. *J. Am. Chem. Soc.* **1983**, *105*, 385.
(8) Hasegawa, A.; Ohnishi, K.; Sogabe, K.; Miura, M. *Mol. Phys.* **1975**, *30*, 1367.
(9) Berclaz, T.; Geoffroy, M.; Lucken, E. A. C. *Chem. Phys. Lett.* **1975**, *36*, 677.
(10) Gillbro, T.; Williams, F. *J. Am. Chem. Soc.* **1974**, *96*, 5032.
(11) Bentrude, W. G.; Moriyama, M.; Mueller, H. D.; Sopchik, A. E. *J. Am. Chem. Soc.* **1983**, *105*, 6053.
(12) Bentrude, W. G.; Rogers, P. E. *J. Am. Chem. Soc.* **1976**, *98*, 1674.
(13) Walling, C.; Pearson, M. S. *J. Am. Chem. Soc.* **1964**, *86*, 2262.
(14) Davies, A. G.; Griller, D.; Roberts, B. P. *J. Organomet. Chem.* **1972**, *38*, C8.
(15) Giles, J. R. M.; Roberts, B. P. *J. Chem. Soc., Perkin Trans. 2* **1981**, 1211.
(16) Janssen, R. A. J.; Visser, G. J.; Buck, H. M. *J. Am. Chem. Soc.* **1984**, *106*, 3429.
(17) Howell, J. M.; Olsen. J. F. *J. Am. Chem. Soc.* **1976**, *98*, 7119.
(18) Ditchfield, R.; Hehre, W. J.; Pople, J. A. *J. Chem. Phys.* **1971**, *54*, 724. Kutzelnigg, W.; Wallmeier, H. *Theoret. Chim. Acta* **1979**, *51*, 261. Schwenzer, G. M.; Schaeffer, H. F. *J. Am. Chem. Soc.* **1975**, *97*, 1393.
(19) Algorithm described by: Fletcher, R. *Comp. J.* **1970**, *13*, 317.
(20) Algorithm described in: *Numerical Methods* for *Nonlinear Algebraic Equations*; Gordon and Breach: London, 1970; Version 1981, p 87.

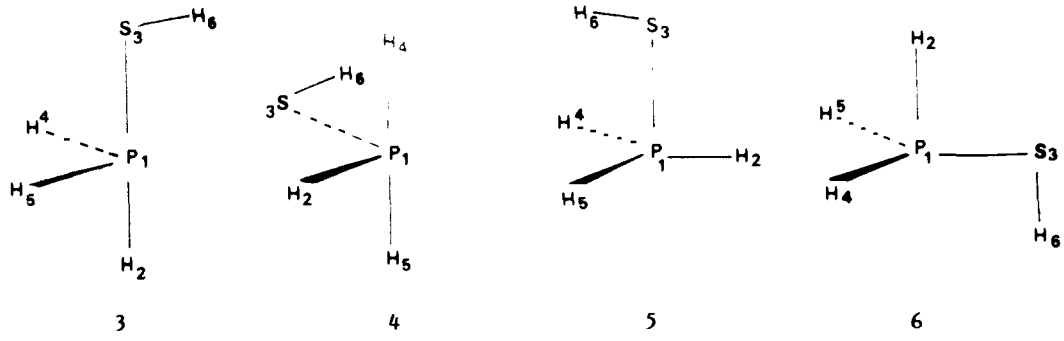

Figure 3. Examined structures for $PH_3(SH)^{\bullet}$.

into account. It is to be noted that the PH_a lengths are much greater than the PH_e lengths for form **1**, while the inverse is observed for form **2** (Figure 1).

In agreement with prior work, we observed a localization of spin density on phosphorus and on the apical ligands in form **1**. On the other hand, in form **2**, we noted a distribution on phosphorus and equatorial ligands (Figure 2). The main contributions are from the p orbital of phosphorus, pointing in the direction of the missing ligand, and the 1s orbitals of the hydrogens. In both case, the contribution from the 3s phosphorus orbital is very weak (0.07).

At the level of overlap populations, whose variation is directly related to that of binding forces, we observed in parallel that values were lower in apical (0.13) than in equatorial directions (0.38) in form **1**. The inverse was observed in the form **2**, i.e., 0.39 in apical and 0.14 in equatorial (Figure 2).

A more detailed analysis at this level in α and β spin, because of the UHF formalism employed, showed that the lowest values were due to the presence of a negative component at −0.04 in α spin in the apical direction in form **1** and in the equatorial directions in form **2**. These negative values arose from antibonding contributions, weakening the corresponding bonds and resulting in the elongations observed in the minimization process. This was seen for apical lengths in form **1** and for equatorial lengths in form **2**. These antibonding contributions participate primarily at the level of the SOMO and involve the 3s orbital of phosphorus and the 1s orbitals of the hydrogens.

3.2. $(PH_3SH)^{\bullet}$ Radical. We carried out a minimization of the $(PH_4)^{\bullet}$ structures considered above: (i) the tetrahedral structure; (ii) the structures deduced from the trigonal bipyramid with a missing ligand either in the equatorial or apical position. Taking the presence of the SH group into account, it corresponds to the four forms shown in Figure 3.

Among the initial five forms, three of them (tetrahedral, **3**, and **6**) do not correspond to any minimum, since in each case we observed a rapid change of the geometric parameters during minimization.

The minimization of form **5** resulted in a single point which we could characterize in a zone of low-energy variation as a point of inflection on the surface (the second derivative was annulled at this point).

The form obtained corresponded to a trigonal bipyramid with a missing apical ligand. We also observed a $H_2P_1S_3H_6$ plane of symmetry for this structure, with one of the hydrogens distinguished from the other two. We noted a longer P_1H_2 bond (1.50 Å) and a considerably decreased $H_2P_1S_3$ angle (82°) (Figure 6).

The atomic spin densities calculated for this entity showed a localization on phosphorus (0.36) and H_2 (0.33). In comparison to the form **2** of $(PH_4)^{\bullet}$ we noted that the apical introduction of SH contributed to a reinforcement of the spin density on phosphorus. The primary contribution to this spin density is that of the p orbital of phosphorus, pointing in the direction of the missing ligand, and whose weighted participation at the level of the SOMO is increased in comparison to that obtained with $(PH_4)^{\bullet}$. This latter comment is consistent with that formulated by Janssen et al.[16] in an investigation of $(PFH_3)^{\bullet}$ in C_{3v} symmetry.

Finally, the minimization of form **4** led to the only structure with a stable arrangement (true minimum) for the $(PH_3SH)^{\bullet}$ radical. It corresponds to a trigonal bipyramid with missing equatorial ligand. The P–H lengths are very close to those determined for the $(PH_4)^{\bullet}$ radical in form **1** (pseudosymmetry C_{2v}), much longer in the apical axis. Similarly, we observed a slight closing of the $H_4P_1H_5$ angle on the side of the missing ligand (Figure 6).

In comparison to the point of inflection, this form is more stable by 45.9 kJ·mol^{-1} (Table II) and a has a deeper SOMO than that of the point of inflection (−8.17 vs. −6.88 eV).

The distribution of spin densities on the apical axis is practically unchanged in comparison to that obtained with $(PH_4)^{\bullet}$ in form **1**. The spin densities on phosphorus are equivalent, and the weighted participation of the 3s orbital phosphorus remains very low (0.08).

In the light of the above results with $(PH_3SH)^{\bullet}$ and on the basis of those obtained with $(PH_4)^{\bullet}$, we attempted to discern why, contrary to **4** and **5**, structures **3** and **6** had no real existence on the surface and rapidly progressed toward dissociation.

In the TBP-e-type structure with apical SH **3** (Figure 4), the examination of overlap populations (in blocked structure, starting point for the minimization) showed a low value of 0.06 for the P–S bond, reflecting a considerable weakening in comparison to the apical P–H bond in form **1** of $(PH_4)^{\bullet}$ (overlap population of 0.13). Decomposition in α and β spins showed a negative component for $(PH_3SH)^{\bullet}$ arising from antibonding contributions involving the 3s orbital of phosphorus and the 3s and 3p orbitals of sulfur. This component was nevertheless on the same order of magnitude for both radicals $(PH_4)^{\bullet}$ and $(PH_3SH)^{\bullet}$, respectively, −0.040 and −0.050. The lower overall values of the overlap population in the case of $(PH_3SH)^{\bullet}$ thus arose from the much lower bonding contributions in this case: 0.11 for $(PH_3SH)^{\bullet}$ and 0.17 for $(PH_4)^{\bullet}$ (lower overlap of phosphorus orbitals with the orbitals of sulfur than with those of hydrogen).

For the TBP-a form with the SH group in equatorial position **6** (Figure 4), we similarly observed an overlap population of 0.04 for the P–S bond, much lower than the value of 0.14 obtained for an equatorial P–H bond in form **2** of the $PH_4^{\bullet}$ radical. Decomposition into α and β spins showed both an increase in the antibonding contributions and a decrease of the bonding contributions. In an overall fashion, this corresponds to a P–S bond which is even weaker than in the TPB-e form (apical SH), reflected by a more rapid progression toward dissociation into PH_3 and $SH^{\bullet}$.

Finally, concerning the tetrahedral form, the very high antibonding contribution along the P–S bond corresponds to considerable instability with immediate elongation of this bond by minimization, leading to rupture.

This structure, suggested by numerous authors when in the presence of third period ligands and considered by Giles and Roberts[15] for $(RSPMe_3)^{\bullet}$, thus does not correspond to the energetically privileged structure. It should be noted that the above authors stated that in view of the ESR measurements, it was not possible to conclude on this point, since they proposed either a Td form or a TBP-e form.

The only minimum obtained corresponds to a TBP-e and presented the SH in equatorial position (overlap population for the PS bond, 0.27). This is in total contradiction to the basic hypotheses of a large body of experimental work concerning

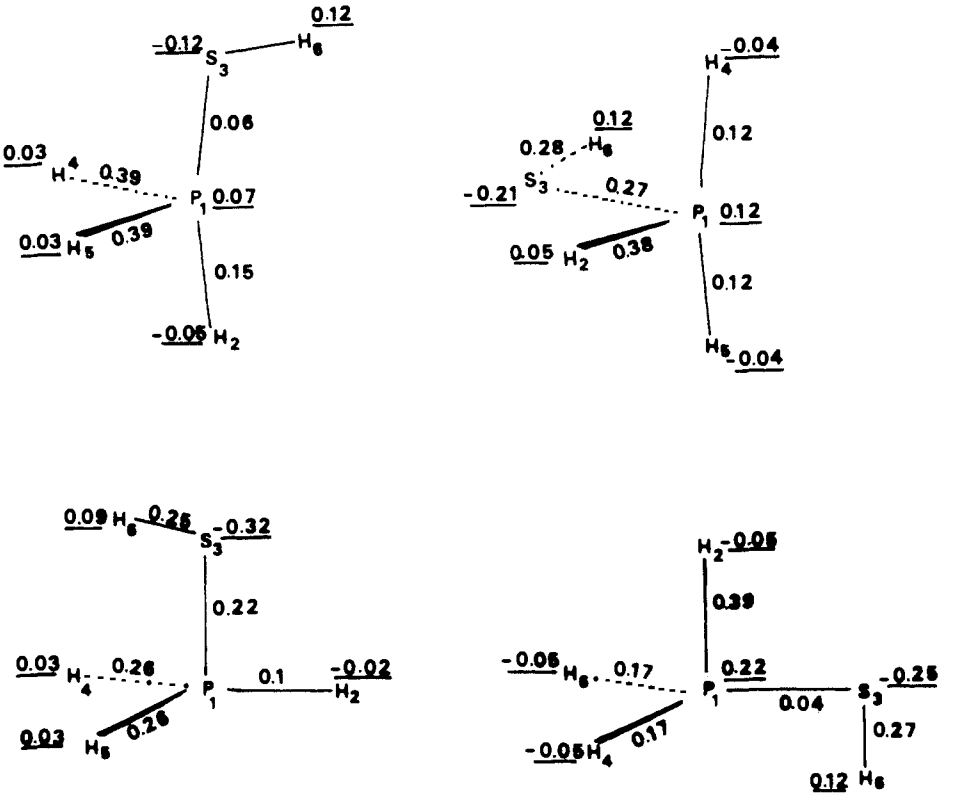

Figure 4. Mulliken populations of **3–6** (net charges underlined).

radicals of the type $(PX_4)^\bullet$, where the most electronegative group is always considered to be in apical position. In a study of $(PF_4)^\bullet$ and $(PF_3H)^\bullet$ Howell[17] observed that equatorial ligands were more negative than axial ligands, in contrast to the case of PX_5 systems. The origin of this difference is the fact that most of the charge on apical atoms arises from the contribution of the last occupied orbital whose weighted participation is much less for a single occupation ($(PX_4)^\bullet$ radicals) than for a double occupation (PX_5 system).

These remarks and the results we obtained on the privileged structure of $(PH_3SH)^\bullet$ thus call into question the formal $(PX_5)(PX_4)^\bullet$ analogies widely used in terms of a preferential position of the most electronegative group in apical position. It would thus seem that, in general, parallels have too often been established between compounds of pentavalent phosphorus and phosphoranyl radicals, which in fact present their own characteristics.

4. Potential Energy Surface of the PH_3 + $SH^\bullet$ System

In order to analyze the mechanism of formation and the possibilities of change of the $(PH_3SH)^\bullet$ radical, we explored the potential energy hypersurface of the system PH_3 + $SH^\bullet$.

4.1. Attack of the $SH^\bullet$ Radical on PH_3. The difference in total energy between the $(PH_3SH)^\bullet$ radical in its preferential structure and that of the isolated minimized species (PH_3, r_{P-H} = 1.405 Å, HPH = 58°; $SH^\bullet$, r_{S-H} = 1.32 Å) is 140.3 kJ·mol^{-1} in favor of dissociation (total energy (PH_3 + $SH^\bullet$) = −739.7430 hartrees, total energy $(PH_3SH)^\bullet$ = −739.6895 hartrees). This comment had been formulated previously for the PH_3 + $H^\bullet$ system. However, we could not affirm if—as previously considered—these results arose from artifacts linked to calculation approximations, since thiyl radicals are generated in situ photochemically with an energy supply in the medium which may lead to the formation of more unstable radicals.

In order to analyze the preferential direction of approach of $SH^\bullet$ to PH_3, we carried out a series of preliminary calculations. Three long distance approaches were considered (directions I–III) (Figure 5).

Direction II is an approach of $SH^\bullet$ along the C_3 axis of PH_3 in the LUMO direction of this system, creating TBP-a apical SH forms. Approach in the HOMO direction (phosphorus pair) of PH_3 (180° opposite in relation to II) appears totally disfavored and will not be analyzed.

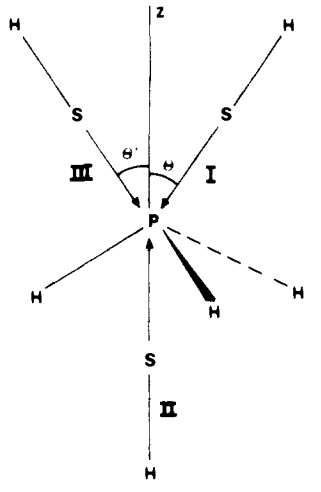

Figure 5. Possible approaches for $SH^\bullet$ attack toward PH_3.

Table I. Energies for $SH^\bullet$ Attack Toward PH_3:[a] Directions I and III, "HOMO Approach"; Direction II, "LUMO Approach"

d_{P-S}, Å	2.9	2.45	2.3
direction I	E = −739.7398	E = −739.7294	E = −739.7200
direction II	E = −739.7143	E = −739.6855	E = −739.6720
direction III	E = −739.7332	E = −739.7216	E = −739.7090
$\Delta(E_{II} - E_I)$	67	115.2	125.8
$\Delta(E_{III} - E_I)$	17.5	20.6	28.7

[a] E = total energy (hartree); ΔE in kJ·mol^{-1}.

Directions I and III are characterized by an angle θ or θ' of about 40° between the entering $SH^\bullet$ and the C_3 axis of PH_3. Changes along these two directions should lead to a TBP-a equatorial SH form for III and to a TBP-e apical SH form for I.

For these three attack directions, we minimized the PH_3 + $SH^\bullet$ system for fixed P–S distances between 2.9 and 2.3 Å, extremes corresponding to the priming of interactions and to the creation

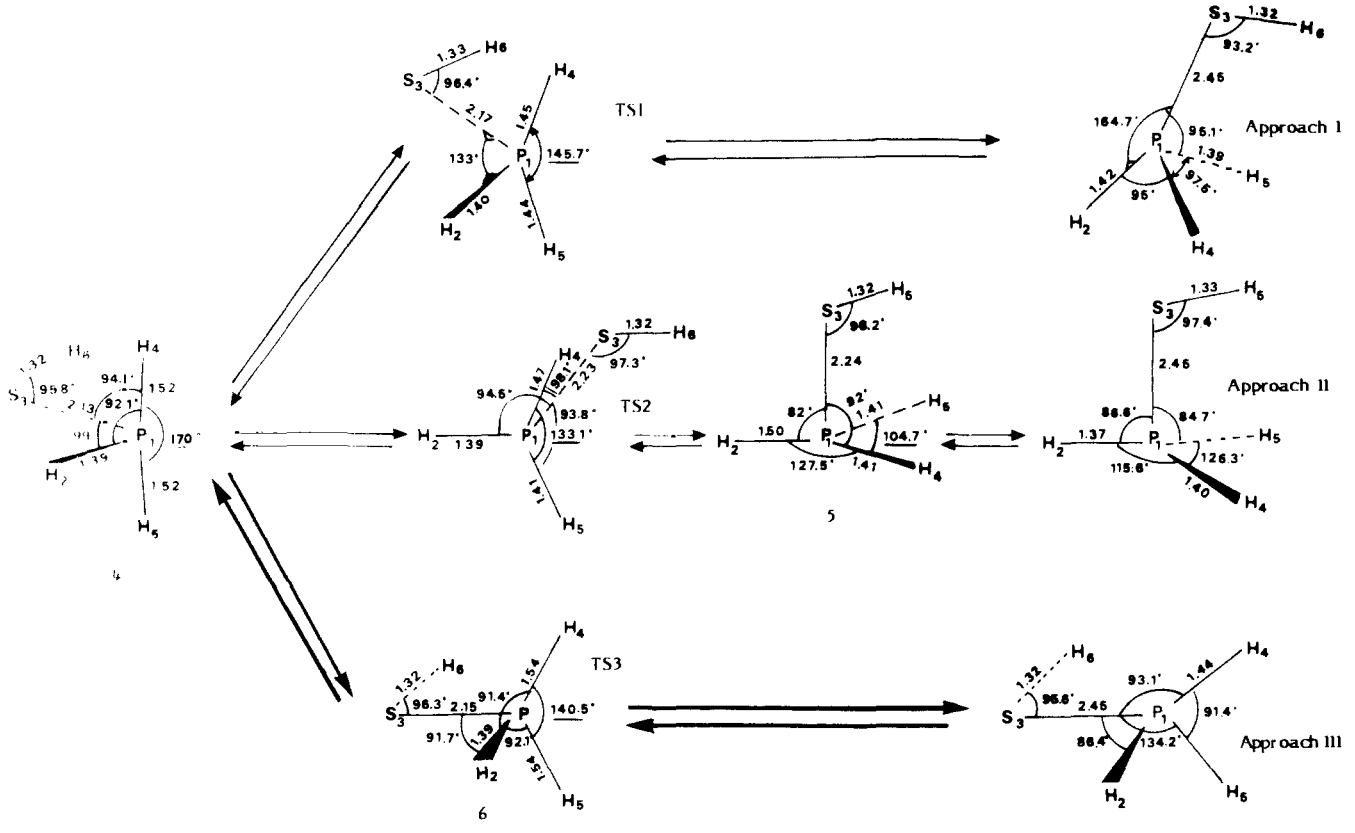

Figure 6. Geometries of $(PH_3SH)^{\bullet}$ on the potential surface (bond lengths in Å).

of a veritable P–S bond. Table I lists the energy values of these supersystems.

These results show that direction II is clearly disfavored in comparison to the other two, excluding an approach of $SH^{\bullet}$ in the LUMO direction of PH_3. Pathways I and III are energetically similar, but I is favored in comparison to III, the energy differences increasing with decreasing P–S length.

At long distances an approach in the apical direction would thus be favored over an equatorial approach. In a study of the $PH_3 + H^{\bullet}$ system, Howell also concluded on this same direction of attack for $H^{\bullet}$ on PH_3, but in this case, equatorial approach was clearly disfavored, in contrast to our observations for the $SH^{\bullet}$ radical.

Figure 6 shows geometries of the $PH_3 + SH^{\bullet}$ system for P–S distances of 2.45 Å. We note that these structures well presage the formation of forms **3**, **5**, and **6**, which are, however, no minima on the potential energy surface. It is thus necessary to invoke pseudorotation mechanisms to reach the only stable structure of the $(PH_3SH)^{\bullet}$ radical: TBP-e with equatorial SH. Inversely, these pseudorotation mechanisms correspond to the different departure possibilities of $SH^{\bullet}$ by α cleavage: (i) departure of the group in apical position, implying a pseudorotation with passage through a TBP-a or TBP-e form with apical SH; (ii) departure of the group in equatorial position. The only possibility in this case, because of the well-established nature of the minimum for the TBP-e (equatorial SH) form, is passage through a TBP-a (equatorial SH) form.

4.2. Mechanisms of Pseudorotation. Pseudorotation mechanisms of PX_5 phosphoranes have been extensively studied. The two classical pseudorotation mechanisms proposed are the Berry rotation[21] and the turnstile mechanism,[22] also invoked for $(PX_4)^{\bullet}$. Thus, a theoretical study of $(PH_4)^{\bullet}$[17] concluded on a higher barrier for the Berry pseudorotation with a C_{4v} transition state than for the turnstile mechanism with a transition state having a TBP-a-type structure. On the bases of experimental data, however, type C_{4v} transition states have most often been suggested to explain the results obtained with phosphoranyl radicals with equivalent ligands.[7]

We have examined the three mechanisms of pseudorotation

TBP-e (equatorial SH) → TS_1 → TBP-e (apical SH)
TBP-e (equatorial SH) → TS_2 → TBP-a (apical SH)
TBP-e (equatorial SH) → TS_3 → TBP-a (equatorial SH)

by evaluating the corresponding barriers.

These saddle points were unambiguously reached by a process of search for extremes, with the determination of the number of associated negative eigenvalues. The geometric structures of the different transition states are shown in Figure 6. The energies of stationary points are listed in Table II.

An attempt was thus made to determine the structure of the transition state in the passage of the privileged TBP-e equatorial SH structure to a TBP-e form with apical SH. The reaction coordinate of this pseudorotation mechanism is the angle θ: $H_2P_1S_3$, which increases from 99° in TBP-e equatorial SH to a

Table II. UHF Energies (hartrees), $\langle S^2 \rangle$ Values, and Index of the Second Derivative Matrix for Structures **1**, **2**, **8**, and **9** and for Stationary Points on $(PH_3SH)^{\bullet}$ Potential Surface

	E(UHF)	$\langle S^2 \rangle$	no. (value) of the neg eigenvalue
form **1**	−342.5801	0.7809	0
form **2**	−342.5503	0.7814	2 (−1.23, −0.55)
$PH_3 + SH^{\bullet}$	−739.7430	0.7557	
form **4**	−739.6895	0.7852	0
TS_1	−739.6598	0.7563	1 (−5.77)
TS_2	−739.6615	0.7602	1 (−2.27)
TS_3	−739.6803	0.7901	1 (−0.97)
form **5**[a]	−739.6717	0.7666	0
TS_4	−739.5900	0.7857	1 (−0.18)
form **8**	−964.0731	0.7620	0
form **9**[a]	−964.0444	0.7613	

[a] The point of inflection was associated with a minimum in the gradient length.

(21) Berry, R. S. *J. Chem. Phys.* **1960**, *32*, 933.
(22) Ugi, I.; Ramirez, F. *Chem. Ber.* **1972**, *8*, 198 and references cited within.

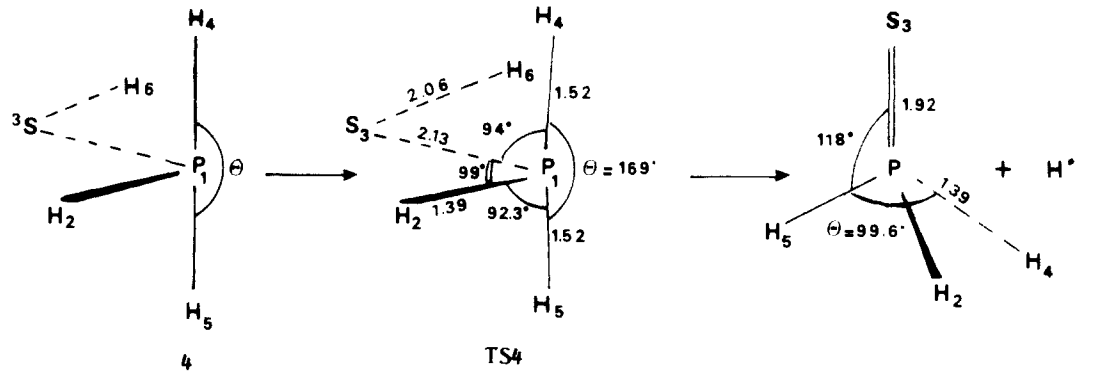

Figure 7. Transition state for β scission of **4** (bond lengths in Å).

value of 133° at the saddle point. In parallel, the angle $H_4P_1H_5$ closes, decreasing from 170° in form **4** to 145.7° in the transition state. Based on its geometric characteristics, this transition state (TS_1) is a deformed tetrahedral structure and not a C_{4v} form, with a lone electron at the pivot, as suggested for certain systems on the basis of experimental findings. The pseudorotation barrier estimated as the difference between the total energies of the TBP-e (equatorial SH) form and the saddle point is 78 kJ·mol^{-1}.

We were able to locate saddle point TS_2 for the rearrangement of TBP-e (equatorial SH) into TBP-a (apical SH). Based on its structural characteristics, this entity is relatively close to a TBP-a with apical SH (Figure 6). The essential coordinate is the angle $\theta = H_4P_1H_5$ which decreases from 170° in TBP-e (equatorial SH), to 133.1° at the saddle point. This angle is closed by maintaining H_2, H_4, and H_5 in the same plane. The angle $H_2P_1S_3$ is only slightly changed. The pseudorotation barrier, estimated as the difference between the total energies of the TBP-e (equatorial SH) form and the saddle point, is 73.6 kJ·mol^{-1}.

Finally, a departure of SH° from an equatorial position led us to seek the pseudorotation saddle point toward a TBP-a equatorial SH form. The geometric parameters are characteristic of a TBP-a equatorial SH form (Figure 6), with the atoms S_3, H_4, and H_5 in the same plane. The reaction coordinate is the angle $H_4P_1H_5$ which is closed in this case from 170° to 140.5°, maintaining S_3, H_4, and H_5 in the same plane. In this case we calculated a weaker barrier of 24.3 kJ·mol^{-1}.

If the energy values of these transition states are examined, it is seen that there are fewer internuclear repulsions in TS_3 than in TS_1, explaining its energy stabilization. In comparison to TS_2, however, the origin of the stabilization of TS_3 is a decrease in the antibonding nature of P–S. Thus, the minimum energy pathway for α cleavage is that which has the lowest pseudorotation barrier, i.e., implying passage from TBP-e (equatorial SH) to TBP-a (equatorial SH). This change appears to be facilitated by the weak barrier.

We thus consider a regeneration of thiyl radicals from the $(PH_3SH)^\bullet$ radical via an α cleavage with the departure of SH° in equatorial position, in contrast to the classical hypothesis of an exclusively apical departure.

So in spite of a preferential pathway I during the approach of SH for P–S distances between 2.9 and 2.3 Å, it appears reasonable, as the minimum energy pathway for the formation of $(PH_3SH)^\bullet$ to propose an initial approach of SH° on PH_3 from an equatorial direction followed by a pseudorotation with passage through the saddle point TS_3.

Experimental work on phosphoranyl radicals has shown that in addition to substitution products (α cleavage), oxidation products can be formed by β cleavage $(PH_3SH)^\bullet \rightarrow H_3P{=}S + H^\bullet$. We extended our approach by examining the formation of thiophosphite.

4.3. Formation of Thiophosphite. In contrast to α cleavage, those of the β type appear to occur primarily for equatorial ligands, based on experimental findings.[4,23] We thus analyzed a β cleavage with the formation of thiophosphite + H°, starting with the energetically privileged form (TBP-e, equatorial SH). However, in light of the structural characteristics of the TBP-a apical SH form, similar to those of thiophosphite, we also examined the departure of an apical H° in this form. It is to be noted that the overlap populations along S–H are practically equivalent for the two structures and so we could not a prior make a selection.

In an initial series of calculations, SH lengths were fixed and chosen to simulate bond breakage, and all other geometric parameters were minimized. This immediately showed that β cleavage could not occur in TBP-a apical SH, since a slight elongation of S–H would cause the P–S bond to break. The mechanistic analysis with TBP-e equatorial SH led to a transition state (TS_4) with a high barrier of 261.2 kJ·mol^{-1}.

We initially observed an elongation of the S–H length, with the other structural parameters remaining unchanged. The structure of this transition state is very close to that of TBP-e equatorial SH, except for the S–H bond, which is 2.06 Å long. Beyond the saddle point, this reaction coordinate participates in tight coupling with the angle $H_4P_1H_5$, which decreases from 170° to 99.6° in thiophosphite (Figure 7).

The thiophosphite + H° system also appears to be slightly favored by 5.5 kJ·mol^{-1} in comparison to TBP-e equatorial SH. In light of these results, the mechanism of β cleavage appears to occur from an equatorial position as suggested experimentally, although the high barrier suggests a rather difficult process for the $(PH_3SH)^\bullet$ radical.

5. $(P(OH)_3SH)^\bullet$ Radical

After determining the preferential structure of the $(PH_3SH)^\bullet$ radical, we investigated $(P(OH)_3SH)^\bullet$ in order to determine the influence of replacing H atoms by OH and thus to verify that the radical chosen ($(PH_3SH)^\bullet$) represented a satisfactory model for interpreting the promoter role of phosphite in photosulfhydratation reactions.

As above, we carried out a minimization of the tetrahedral structure and of the TBP-e and TBP-a forms **7** to **10** (Figure 8).

As the result of the very large size of the systems, it was not possible to minimize all geometric parameters. The values of some of them were set (values in parentheses in the geometries presented), but rotation of OH and SH around the P–O and P–S bonds was permitted.

As we observed in the case of $(PH_3SH)^\bullet$, the minimization of three of the five forms examined (Td, **7**, and **10**) led to the dissociation into $P(OH)_3$ and SH° via "loose complexes" of the same type as those previously obtained. We were also able to observe a more rapid modification of geometric parameters for the Td form than for form **10**; form **7**, located in a zone of relatively low-energy variation, progressed more slowly. These behaviors are entirely analogous to those observed in the case of $(PH_3SH)^\bullet$, although the progression of all the geometric parameters is slower.

For the other two structures, **8** and **9**, the results show that form **8** was energetically favored by about 75.27 kJ·mol^{-1} in comparison to form **9** (total energy (form **8**) = −964.0731 hartrees, $\langle S^2 \rangle$ = 0.7620, total energy (form **9**) = −946.0444 hartrees, $\langle S^2 \rangle$ = 0.7613). The latter form appears to correspond to a point of

(23) Davies, A. G.; Griller, D.; Roberts, B. P. *J. Chem. Soc., Perkin Trans. 2* **1972**, 2224.

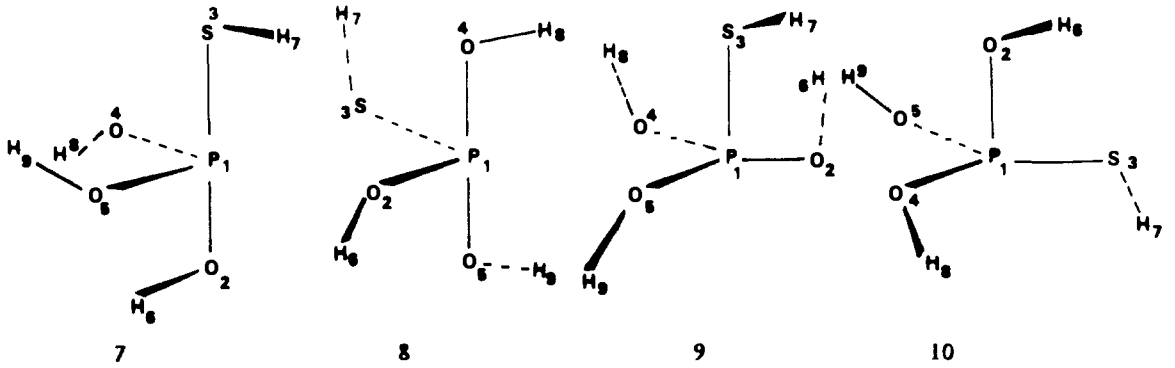

Figure 8. Examined structures for $(P(OH)_3SH)^*$.

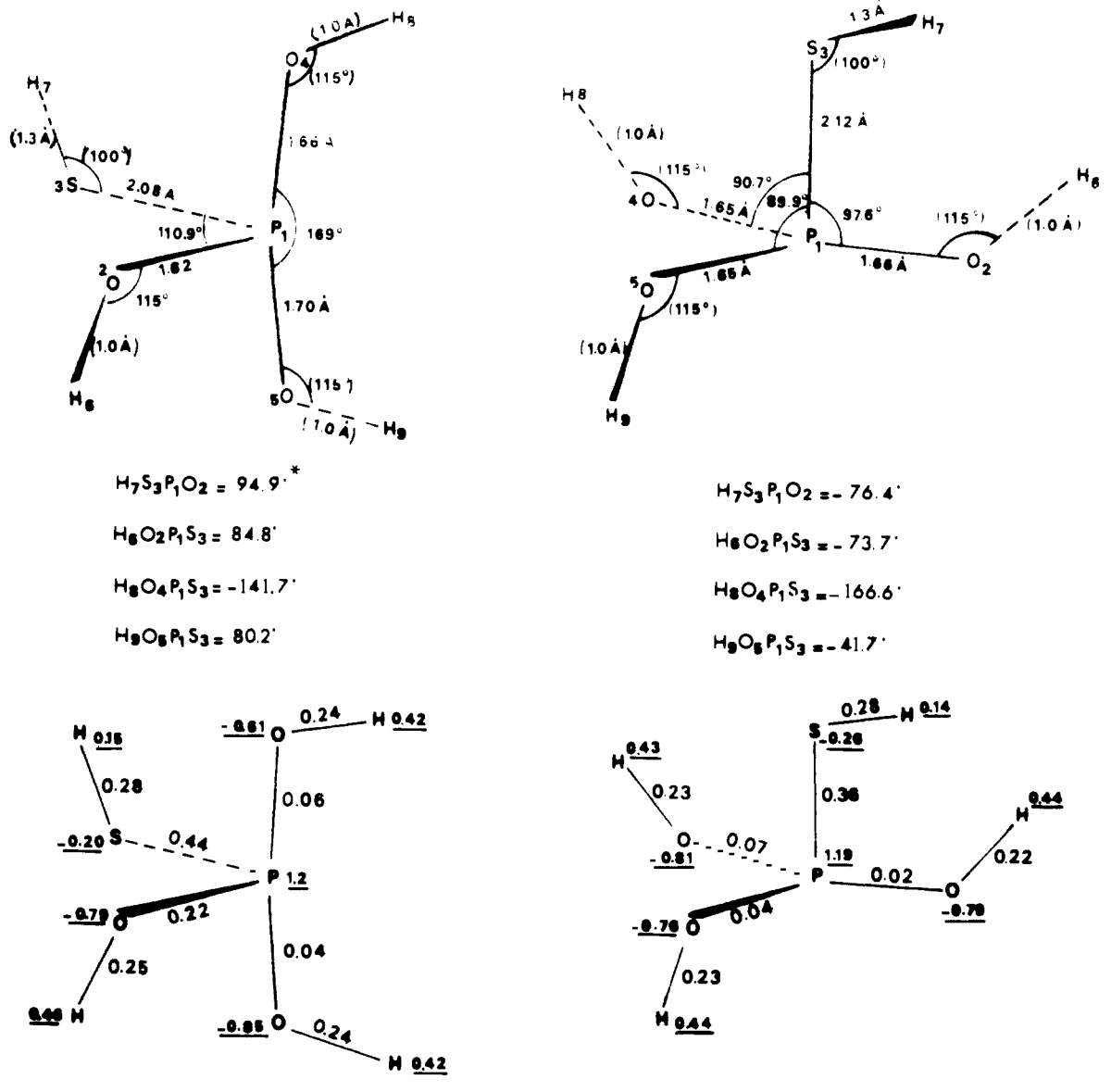

* Dihedral angle NABC - looking along bond from A to B, C is atom that dihedral angle is measured from (in counterclockwise direction)

Figure 9. Optimized geometries and Mulliken populations (net charges underlined) of 8 and 9.

inflection on the surface, although it was not characterized with as much precision as in the case of $(PH_3SH)^*$, because of the time required for the calculation. Nevertheless, the most important point is the fact that the TBP-e form with equatorial SH, whicl corresponds to the energetically privileged structure for $(PH_3SH)^*$ is also favored in the case of $(P(OH)_3SH)^*$.

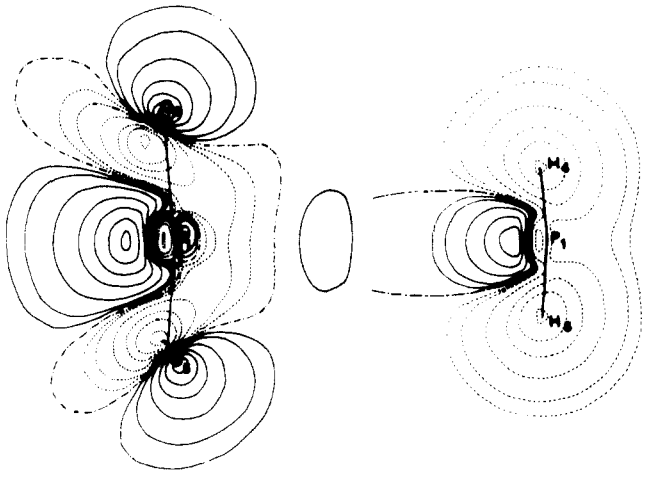

Figure 10. Wave function contours of the SOMO for **8** and **4**: contours are 0.3 ± 0.25 − 0.2 ± 0.15 ± 0.1 ± 0.05 ± 0.02 ± 0.01 (electron $bohr^{-3})^{1/2}$; positive values are indicated by solid lines.

Aside from these energy considerations, it was of interest to examine the modifications of geometric parameters, spin densities, and the Mulliken populations induced by passing from $(PH_3SH)^\bullet$ to $(P(OH)_3SH)^\bullet$ for the two characteristic structures, i.e., for the TBP-a apical SH form (point of inflection) and for the TBP-e SH equatorial form (only minimum obtained). For the forms called TBP-a apical SH **5** and **9** (Figure 9), we observed similar P–S bond lengths. Although one of the P–O bonds was always distinguished from the other two in form **9**, this was less clear-cut for the P–H bonds, of which one appeared clearly differentiated in form **5**.

On the other hand, greater modifications affected spin density distribution, almost totally localized on phosphorus in $(P(OH)_3SH)^\bullet$ with a value of 0.72, much higher than the value of 0.36 obtained with $(PH_3SH)^\bullet$. An analysis of orbital contributions in the case of $(P(OH)_3SH)^\bullet$ showed 0.27 for the 3s orbital of phosphorus and 0.45 for the 3p orbital of the same atom. Thus, the presence of OH ligands in this type of structure contributes to a clear reinforcement of the weighted participation of the 3s(P) orbital, which was only 0.08 in the case of $(PH_3SH)^\bullet$. These results are to be compared to those obtained by Janssen[16] in a comparative examination of $(HPH_3)^\bullet$ and $(HPF_3)^\bullet$ in C_{3v} structure, where a similar increase was observed.

Concerning the TBP-e equatorial SH forms **4** and **8** (Figure 9), the greatest structural changes involve a 10° opening of the angle between the equatorial ligands in $(P(OH)_3SH)^\bullet$ and the dissymmetry which appeared in the two apical bond lengths of the OH ligands. On the other hand, the P–S bond length and the $H_4P_1H_5$ or $O_4P_1O_5$ angles were very close in the two structures.

Furthermore, the spin densities of forms **4** and **8** were clearly different. In the case of $(P(OH)_3SH)^\bullet$ and in contrast to the results obtained with $(PH_3SH)^\bullet$ the greatest contribution was that of phosphorus (0.29 in form **4** and 0.67 in form **8**). This phenomenon is visualized in the SOMO plot of the $(P(OH)_3SH)^\bullet$ radical in the $O_4P_1O_5$ plane (Figure 10). In comparison to a similar plot obtained with $(PH_3SH)^\bullet$, the localization of the unpaired electron is much greater on phosphorus.

In addition, the examination of orbital participations in **8** reveals values of 0.23 and 0.44 for the 3s and 3p orbital of phosphorus, entirely reasonable results in light of the experimental data obtained for TBP-e systems with apical oxygen atoms[7] (0.22–0.24 for the 3s orbital, 0.47–0.49 for the 3p orbital).

Among the Mulliken populations, forms **8** and **9** have highly negative oxygen atoms and a phosphorus which is much more positive than in forms **4** and **5** of the $(PH_3SH)^\bullet$ radical. The overlap populations are the reflection of P–O bonds which are weaker than P–H bonds, although there is a reinforcement of the P–S bond in the case of OH ligands.

The $(P(OH)_3SH)^\bullet$ radical thus has considerable structural analogy with the $(PH_3SH)^\bullet$ radical. The privileged structure is a TBP-e form with equatorial SH, a conclusion which is difficult to predict a prior in light of the results obtained with $(PH_3SH)^\bullet$ and because of the fact that the apicophilic natures of the ethoxy and ethylthio groups had been estimated to be on the same order, on the basis of experimental findings.[24]

6. Conclusion

This overview analysis of the potential energy hypersurface of the $PH_3 + SH^\bullet$ system brings out a number of points, partially negating the generalizations deduced from the $(PH_4)^\bullet$ model:

The TBP-e equatorial SH form **4** is the only stable structure of the radical.

The TBP-e apical SH form **3** has no extreme (minimum or saddle point).

The TBP-a apical SH form **5** participates on the surface as a point of inflection.

The TBP-a equatorial form **6** appears as the saddle point of the process of radical dissociation, leading to the regeneration of $SH^\bullet$.

Finally highly deformed tetrahedral structures were characterized as saddle points in pseudorotation mechanisms.

The partial results obtained for OH ligands showed analogies between the two radicals. The preferential structure also corresponds to a TBP-e with equatorial SH. The participation of phosphite as a promoter in photosulfhydratation reactions is intimately related to the formation of this radical: its change in the presence of ethylenic compounds is the problem we are addressing based on the above data.

Acknowledgment. This work was supported by Société Nationale Elf-Aquitaine (Production).

Registry No. $(PH_3SH)^\bullet$, 102780-10-9.

(24) Brierley, J.; Trippett, S.; White, M. W. *J. Chem. Soc., Perkin Trans. 2* **1977**, 273.